C. R. Chimie 19 (2016) 1631–1641

Contents lists available at ScienceDirect

Comptes Rendus Chimie

www.sciencedirect.com

Full paper/Mémoire

Detection of silica and calcium carbonate deposits in granulomatous areas of skin sarcoidosis by μFourier transform infrared spectroscopy and Field Emission Scanning Electron Microscopy coupled with Energy Dispersive X-ray Spectroscopy analysis

Hester Colboc [a, *], Dominique Bazin [b, c], Philippe Moguelet [a], Vincent Frochot [d, e], Raphaël Weil [c], Emmanuel Letavernier [d, e], Chantal Jouanneau [d], Camille Francès [f, g], Claude Bachmeyer [h], Jean-François Bernaudin [a, g, i], Michel Daudon [d, e]

[a] AP-HP, Hôpital Tenon, Anatomie et Cytologie Pathologiques, 75020 Paris, France
[b] Sorbonne Universités, UPMC Université Paris-6, CNRS, Collège de France, Laboratoire de Chimie de la Matière Condensée de Paris, 11, place Marcelin-Berthelot, 75005 Paris, France
[c] CNRS, LPS, Bât. 510, Université Paris-11, 91405 Orsay, France
[d] AP-HP, Hôpital Tenon, Explorations Fonctionnelles Multidisciplinaires, 75020 Paris, France
[e] Sorbonne Universités, UPMC Université Paris-6, UMR S 1155, 75005, Paris France
[f] AP-HP, Hôpital Tenon, Dermatologie, 75020 Paris, France
[g] Sorbonne Universités, UPMC Université Paris-6, 75005 Paris, France
[h] AP-HP, Hôpital Tenon, Médecine Interne, 75020 Paris, France
[i] Groupe SILICOSIS, Sciences Po, 75007 Paris, France

ARTICLE INFO

Article history:
Received 15 March 2016
Accepted 10 May 2016
Available online 9 June 2016

Keywords:
Sarcoidosis
Granulomas
Infrared spectroscopy
Field Emission Scanning Electron Microscopy
Energy Dispersive X-ray Spectroscopy
Silica
Calcium carbonate

ABSTRACT

Sarcoidosis is a multisystem inflammatory disease affecting different organs particularly lung, skin, eyes and joints. Characterized by noncaseating epithelioid granulomas, sarcoidosis is considered to be caused by a complex interplay between genetics and environmental agents while it still remains a disease of unknown etiology. 10 skin biopsies from patients with cutaneous sarcoidosis were included in the study. After polarized light examination (PLE) through optical microscopy, these skin biopsies have been investigated through μFourier transform (FTIR) infrared spectroscopy and Field Emission Scanning Electron Microscopy coupled with Energy Dispersive X-ray Spectroscopy (FE-SEM/EDX). Three biopsies showed a refractive material at PLE. FTIR and FE-SEM/EDX analyses indicate the presence of silica at the center of the granulomas in these three biopsies. Another striking result is related to the presence of calcite, a calcium carbonate at the periphery of the granulomas. To our best knowledge, this is the first time that the presence of this calcium carbonate has been reported. Such description at the submicrometer scale paves the way for a better understanding of the physicochemical processes related to sarcoidosis and will help clinicians to develop new diagnostic tools.

* Corresponding author.
E-mail address: hestercolboc@gmail.com (H. Colboc).

http://dx.doi.org/10.1016/j.crci.2016.05.007

1. Introduction

Sarcoidosis is a multisystem granulomatous disease affecting the skin in 25–30% of cases reported in [1]. Cutaneous lesions are widely variable; papular sarcoidosis, annular sarcoidosis, maculopapular eruption and lupus pernio are more common [2]. Disease onset peaks during the third and fourth decades of life have a higher incidence among women and are seen more frequently in Blacks than in Caucasians [2]. Sarcoidosis is characterized by non-caseating epithelioid and giant cells granulomas, the hallmark of the disease. The granulomatous inflammation observed in sarcoidosis is thought to be caused by a complex interplay between a genetic background, environmental agents, infectious antigens and T lymphocyte immune reactions [3].

Cutaneous sarcoidosis preferentially affects sites with a prior injury such as tattoos or scars and a polarizable material has been reported in almost 25% of cases suggesting that foreign materials could be a nidus for granuloma formation and a potential trigger for the disease [4–7].

Sarcoidosis, as observed in other granulomatous diseases, is associated with calcium metabolism disorders. High serum calcium is seen in 5–10% of patients [8], mainly due to a dysregulated production of calcitriol by activated macrophages forming the granulomatous lesions [9]. These metabolic disturbances may lead to deposit of calcium in various organs, including the skin, as seen in calcinosis cutis [10].

Sarcoidosis is a disease of which the causes are still unknown, although the role of environmental mineral particles is strongly suspected on the grounds of epidemiological data [11,12]. Nowadays, there are increasing interest and recent developments in nanotechnology in order to understand the effects of nanoparticles on living tissues [13]. Therefore, the importance of morphology and chemical analysis of pathological calcifications has been clearly underscore in different organs but never recognized in sarcoidosis [14–17]. The present study has been designed to investigate the physico-chemical characteristics of 1) intragranuloma polarizable foreign materials and 2) tissue deposits in biopsy samples of 10 cutaneous sarcoidoses. In order to describe their structural characteristics as well as their chemical nature at the subcellular scale, two different techniques were used: Field Emission Scanning Electron Microscopy coupled with Energy Dispersive X-ray Spectroscopy (FE-SEM/EDX) [18–20] and μFourier Transform Infra-Red (μFT-IR) [21–27] spectroscopy.

2. Material and methods

2.1. Patients

Ten samples of formalin fixed, paraffin embedded biopsies from cutaneous sarcoidosis patients, stained with hematoxylin and eosin (H&E), were retrieved from the Pathology Department of Hôpital Tenon APHP Paris (Pr I. Brochériou). Sarcoidosis patients were followed in the Dermatology Department (Pr C. Francès) or the Internal Medicine Department (Dr C. Bachmeyer) of Hôpital Tenon APHP Paris. The diagnosis of sarcoidosis has been made on clinical data and histopathology results [4]. In accordance with French legislation, no written informed consent was necessary. Clinical characteristics of patients and histopathology of biopsies are summarized in Table 1.

The first stage of this investigation employed optical microscopy and PLE analysis.

2.2. FTIR microspectroscopy

FT-IR data were used to localize and determine the chemical nature of the pathological deposits in the skin biopsies. As discussed in previous reports [20,23], skin biopsies were deposited on low-e microscope slides (MirrIR, Kevley Technologies, Tienta Sciences, Indianapolis). All the FT-IR hyperspectral images were recorded with a Spectrum Spotlight 400 FT-IR imaging system (Perkin Elmer Life Sciences, France), with a spatial resolution of 6.25 μm and a spectral resolution of 8 cm^{-1}. Each spectral image, covering a substantial part of the biopsy, consisted of about 30,000 spectra. All biopsies presumed to contain crystal deposits were analyzed with the Spotlight 400 FTIR imaging System in the mid

Table 1
Skin biopsies analyzed: clinical characteristics of the patients and histopathology.

n	Patient		Clinical presentation[b]		Biopsy		
	Age	Gender[a]	Site	Morphology	Site	Granulomas location	PLE[c]
1	69	M	Toes	Papules	Toe	Superficial and deep dermis	Negative
2	43	F	Nose Upper limb	Angiolupoid Plaque	Elbow	Superficial and deep dermis	Positive
3	31	M	Temple	Annular lesion	Temple	Superficial and deep dermis	Negative
4	42	M	Upper limbs Tattoo	Papules	Upper limb	Superficial dermis	Positive
5	42	M	Back	Papules	Back	Superficial and deep dermis	Negative
6	61	F	Upper limbs	Papules	Upper limb	Deep dermis and subcutis	Negative
7	49	M	Lower limbs	Papules	Lower limb	Subcutis	Negative
8	54	M	Lower limbs	Nodules	Lower limb	Deep dermis and subcutis	Negative
9	23	F	Forehead	Papules	Forehead	Superficial and deep dermis	Positive
10	21	H	Lip	Macro-cheilitis	Lip	Superficial and deep dermis	Negative

[a] M: male; F: female.
[b] Clinical presentation of the cutaneous lesions.
[c] PLE: polarized light examination.

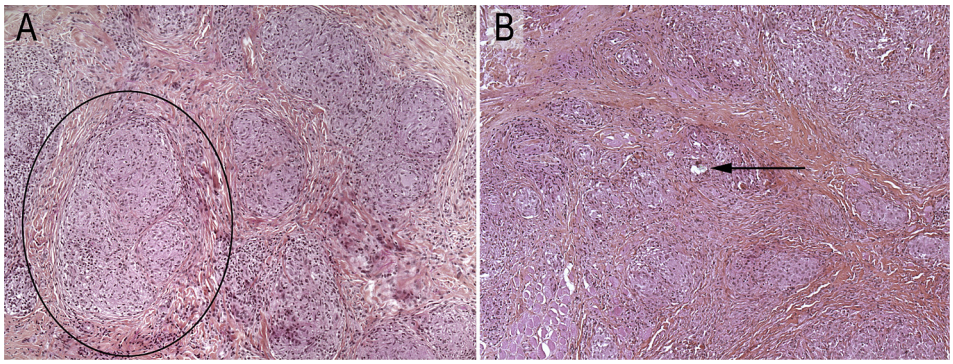

Fig. 1. Typical granulomas (black circle) without (A) and with (B) birefractile bodies (arrow) (H&E ×100).

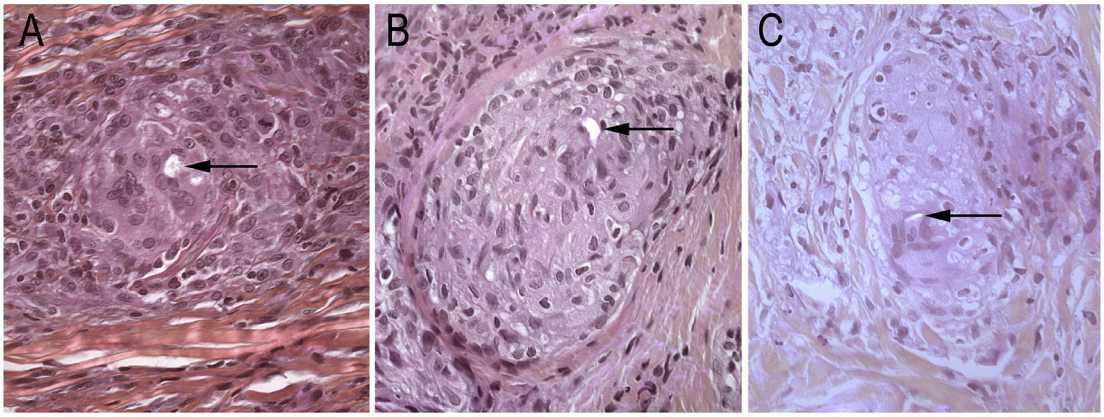

Fig. 2. Samples Nos. 9 (A), 2 (B) and 4 (C) in PLE (H&E magnification ×400) showing birefringent bodies in the granulomas (arrows).

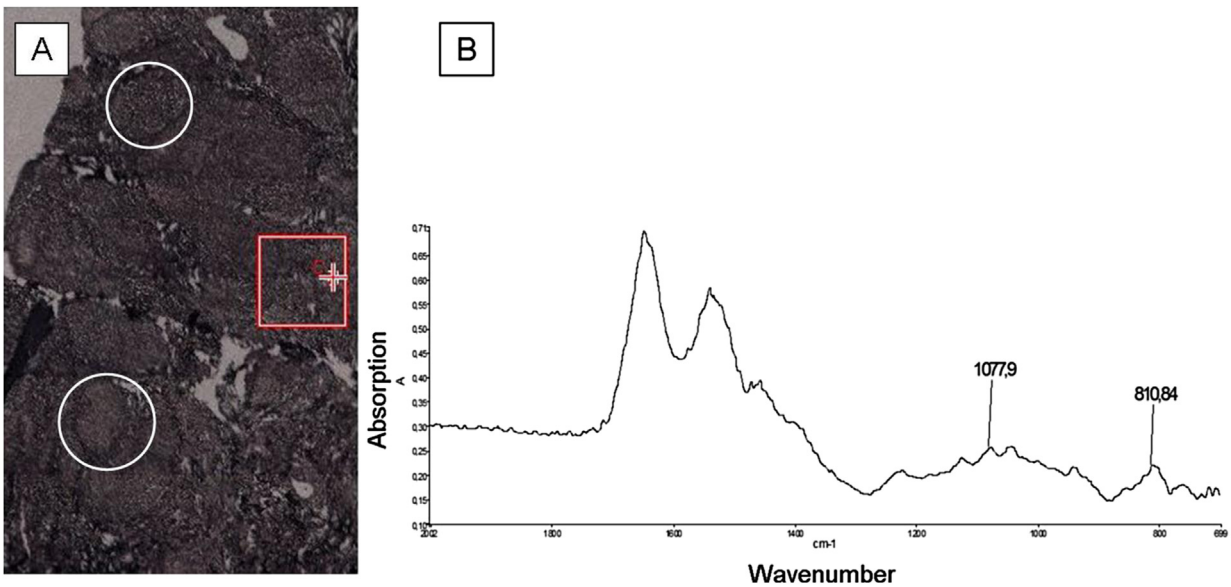

Fig. 3. (A) Optical photograph of sample No. 2 (white circles indicate granulomas); (B) IR spectrum of the protein matrix from the region corresponding to the red cross on the map, located in the dermis, showing the characteristic signals of silica in the protein matrix.

infrared (4000–700 cm^{-1}) spectral range to obtain infrared maps of tissue slides at high spatial resolution, down to 10 microns.

2.3. Field Emission Scanning Electron Microscopy

All the FE-SEM observations were performed on a Zeiss SUPRA55-VP SEM. Such a field-emission "gun" microscope operates either at 1 or 2 kV. High-resolution observations were obtained by 2 secondary electron detectors: an in-lens SE detector and an Everhart–Thornley SE detector [18,20]. The measurements were taken at low voltage (between 0.5 and 2 kV) without the usual deposits of carbon at the surface of the sample. For some samples, an Energy Dispersive X-ray (EDX) experiment was also performed to identify calcium in the abnormal deposits.

3. Results and discussion

3.1. Optical microscopy and polarized light examination

In all the 10 biopsies analyzed, characteristic epithelioid and giant cell granulomas were observed in the dermis and subcutis (Fig. 1A and B).

In most of them (8/10) more than 10 granulomas per section were observed. After Polarized Light Examination (PLE), the refractive material was detected in 3/10 biopsies restricted to one or two granulomas among the numerous granulomas present (Fig. 2; Table 1).

3.2. FTIR spectroscopy

FT-IR microspectroscopy analysis was then used in order to detect, localize and determine the chemical nature of deposits in the 10 skin biopsies. This method has been

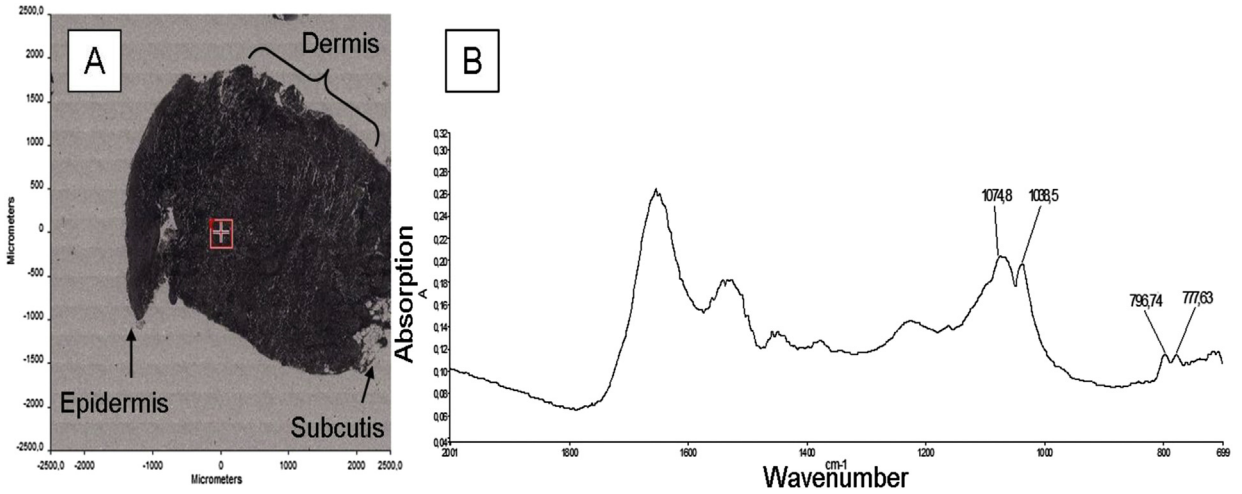

Fig. 4. (A) Optical photograph of the sample No. 4; (B) IR spectrum of crystalline silica with the characteristic peaks in a protein matrix, corresponding to the red cross on the map, located in the dermis.

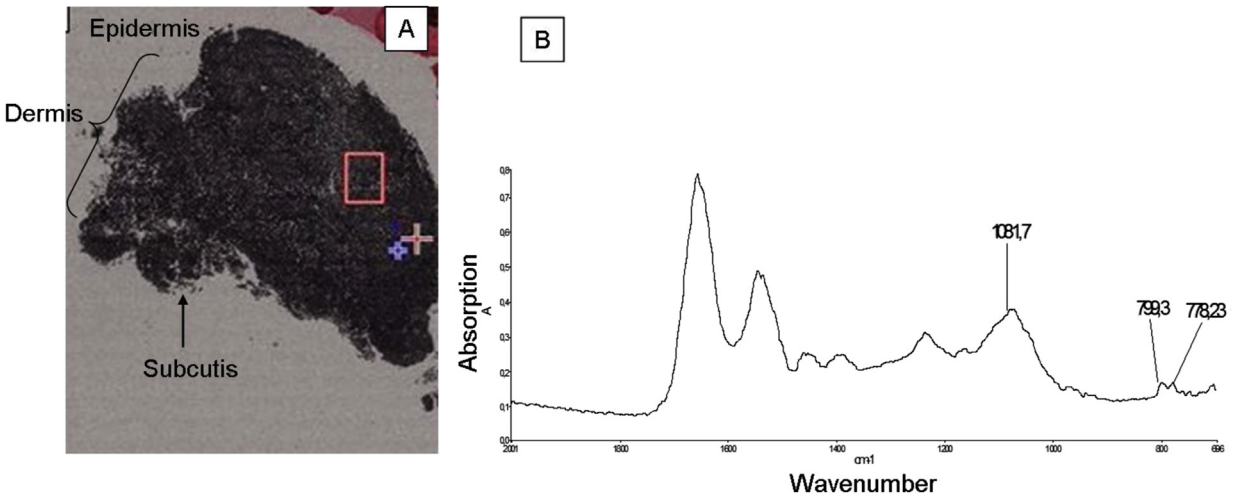

Fig. 5. (A) Optical photograph of the sample No. 9; (B) FT-IR spectrum corresponding to the red square on the map.

shown to be particularly valuable for chemical analysis of living tissues and recent experimental developments in FTIR microspectroscopy have allowed the collection of FT-IR spectrum at the nanometer scale [28–30].

3.2.1. Normal epidermal and dermal tissue structures

In a typical FT-IR, components of the skin which absorb in the infra-red range, can give rise to typical signatures. For example, a portion of the IR signal arises from collagen which is a major structural protein in the skin (type I and III) and plays a key role in providing structural scaffolding. Indeed, the collagen fibrils can be visualized through amide I (at 1660 cm^{-1}), methylene (CH_2 at 1450 cm^{-1}) and amide III (at 1260 cm^{-1}) [31]. Significant results have also been obtained regarding the spatial distribution of lipids in the human stratum corneum using an experimental setup combining an atomic force microscope and a tunable IR laser source [32]. Using the absorbances at 2930 cm^{-1} (lipid) and 3290 cm^{-1} (keratin), the data collected by C. Marcott et al. [32] suggest that regions of higher lipid concentration are located at the perimeter of corneocytes in the normal stratum corneum.

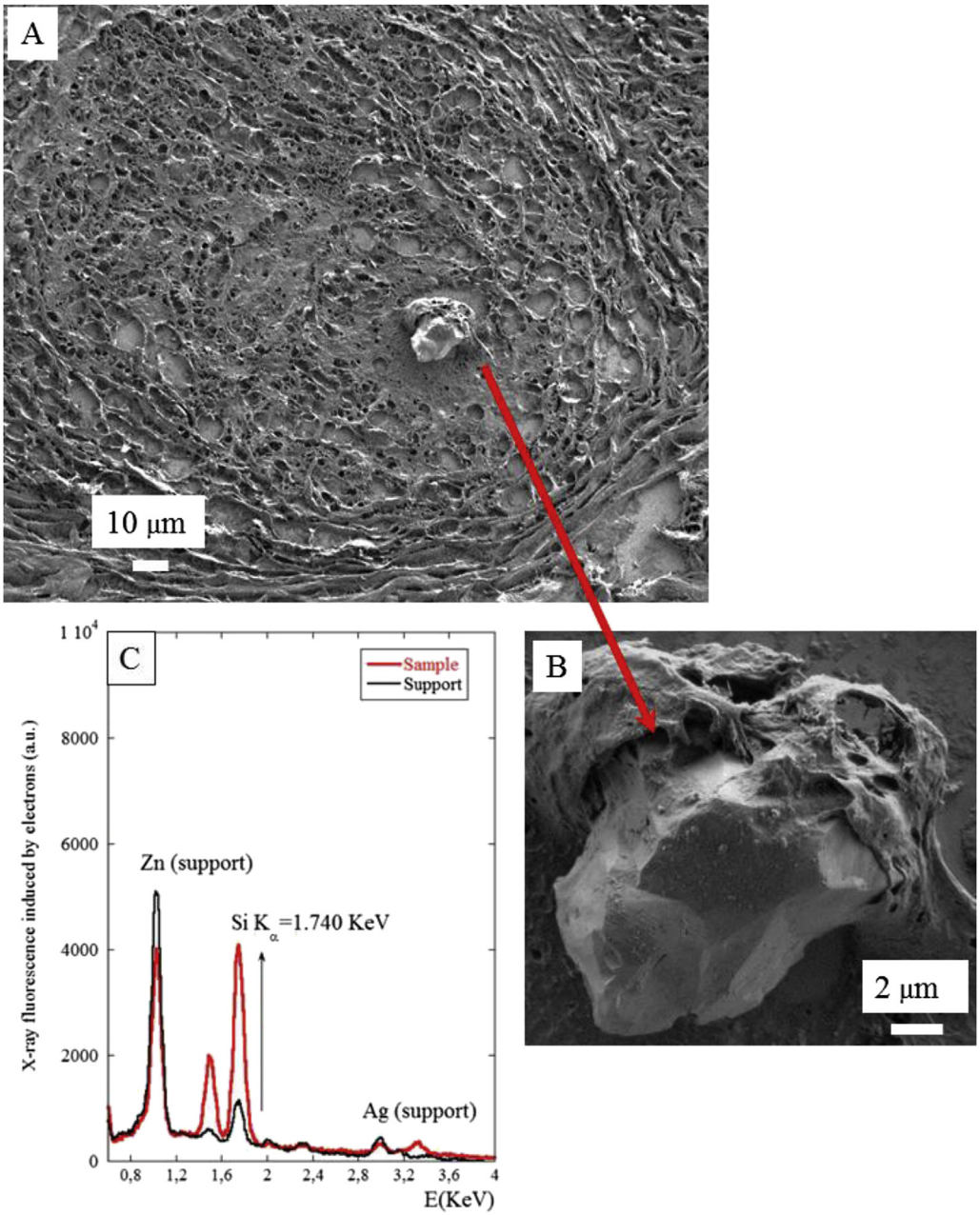

Fig. 6. (A) and (B) SEM photographs of sample No. 2 at two magnifications. (A) The abnormal deposit is clearly shown in the center of the granuloma. (C) The EDX spectrum identifies the presence of silicon in the abnormal deposit present at the center of the granuloma.

3.2.2. Abnormal deposits in granulomas

Based on previous investigations performed on abnormal deposits in granulomas and following our polarized light examinations we suspected the presence of silica confirmed by FTIR spectroscopy.

As reported by Lippincott et al. [33], three frequencies around 1100, 800, and 480 cm^{-1} are characteristic of all the polymorphs of SiO_2. These frequencies respectively correspond to a stretching mode involving displacements associated primarily with the oxygen atoms, a stretching mode involving displacements associated primarily with the silicon atoms, and a Si—O bending mode. Note that silica exists in many different polymorphs, α and β-quartz, α and β-cristobalite, coesite, stishovite and a $CaCl_2$-like form, each one thermodynamically stable in a different region of the phase diagram [34,35]. The most stable phase of silica under ambient conditions is α-quartz, which belongs to the class of silica structures with corner-sharing

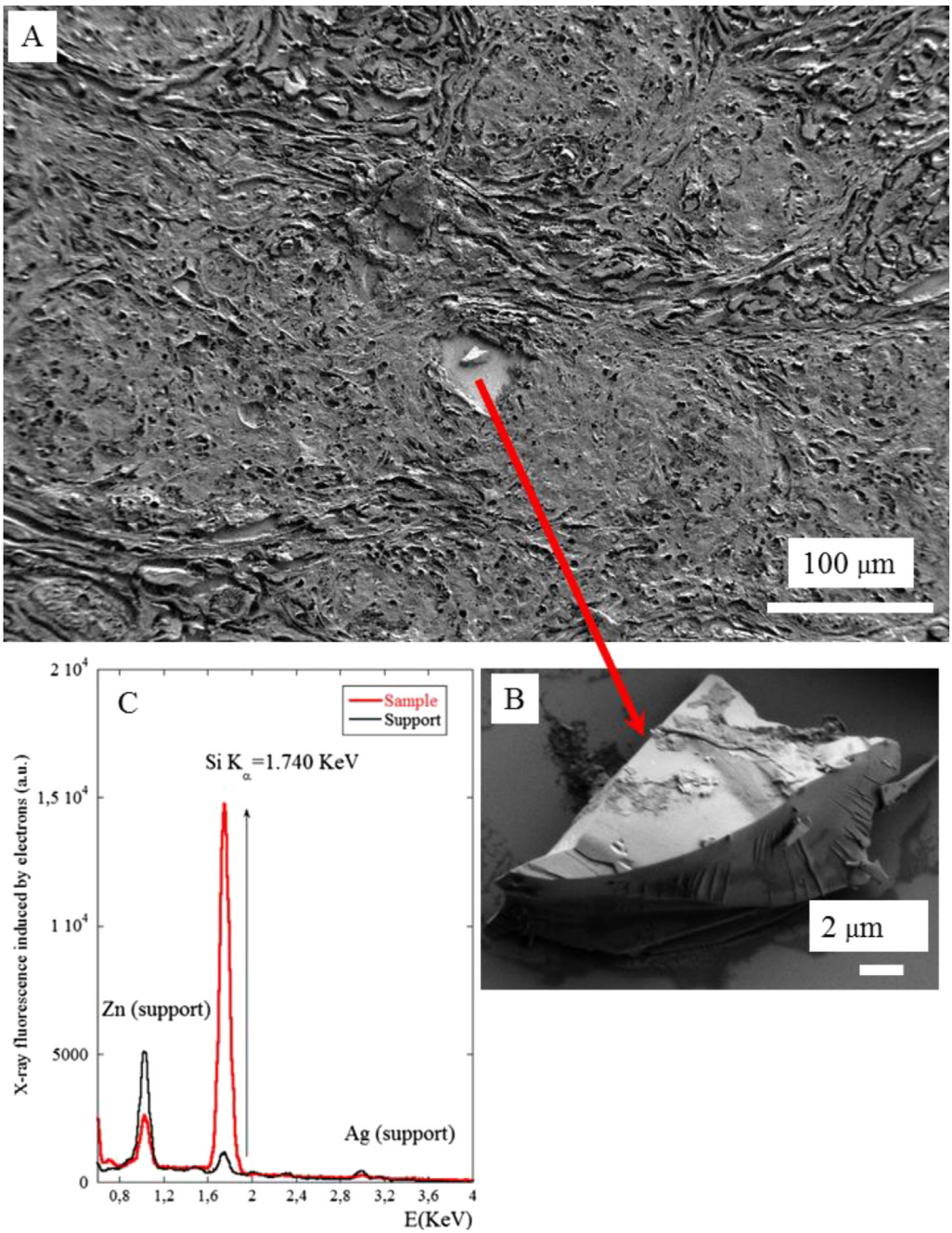

Fig. 7. (A) And (B) SEM photographs of sample No. 4 at two magnifications (C) The EDX spectrum shows the presence of silicon in the chemical composition of the abnormal deposit present in the center of the granuloma.

SiO_4 tetrahedra. It is worth stressing that such polymorphism may be significant from a medical point of view. Recently, K.M.A. O'Reilly et al. [36] have reported that crystalline silica and amorphous silica differentially regulate the cyclooxygenase-prostaglandin pathway in pulmonary fibroblasts.

Fig. 3A shows an optical image of sample No. 2 which corresponds to the superficial dermis containing many granulomas. Signals at 810 and 1078 cm^{-1} correspond to a silica species.

Fig. 4A shows an optical image of sample No. 4 which corresponds to the epidermis, dermis and part of the subcutis, in which the different absorption bands at 1072 and 1036 cm^{-1} are associated with crystalline silica.

Finally, Fig. 5A, shows an optical image of sample No. 9 corresponding to the three layers of the skin, with granulomas, in this sample, located in the dermis. The doublet absorption bands at 799 cm^{-1} and 776 cm^{-1} due to the Si—O—Si intertetrahedral bridging bonds in α-quartz are clearly visible in this sample.

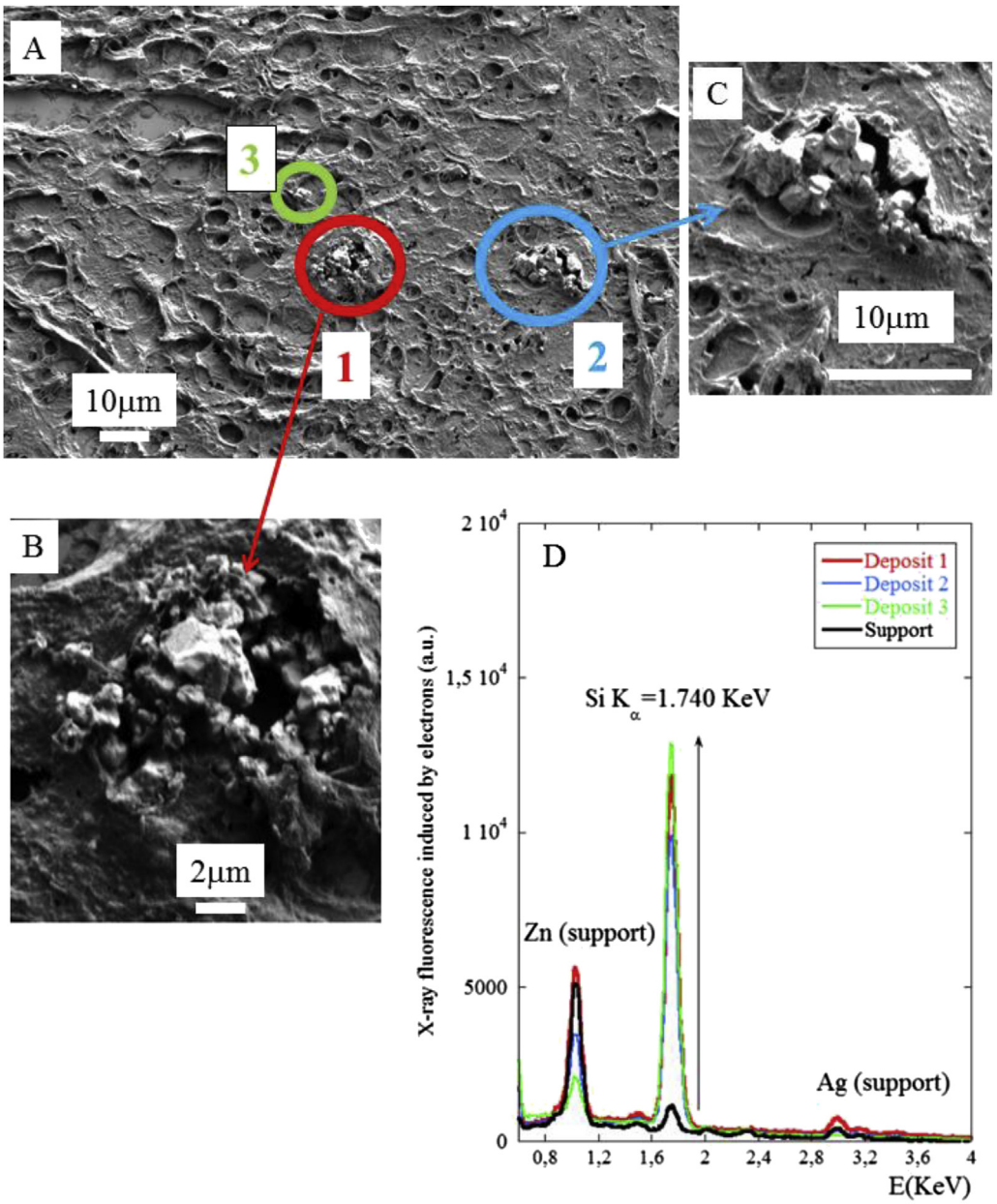

Fig. 8. (A), (B) and (C) SEM photographs of sample No. 9 at two magnifications (D) The EDX spectrum shows the presence of silicon in the abnormal deposit in the center of the granuloma. Zn and Ag are present on the sample support.

3.3. FE-SEM/EDX analysis

FE-SEM/EDX observations enable us to characterize the location of these abnormal deposits at the micrometer scale. The three skin layers are recognizable on the FE-SEM microphotographs: the superficial layer (50–100 μm), composed of epidermis and stratum corneum, the dermis (1–2 mm) and the subcutis (1–2 mm). We first focussed on the intragranuloma silica deposits, and secondly the Ca carbonate deposits.

3.3.1. Intragranuloma silica deposits

The 3 samples with refractive material detected by PLE were investigated by FE-SEM/EDX analysis. Results

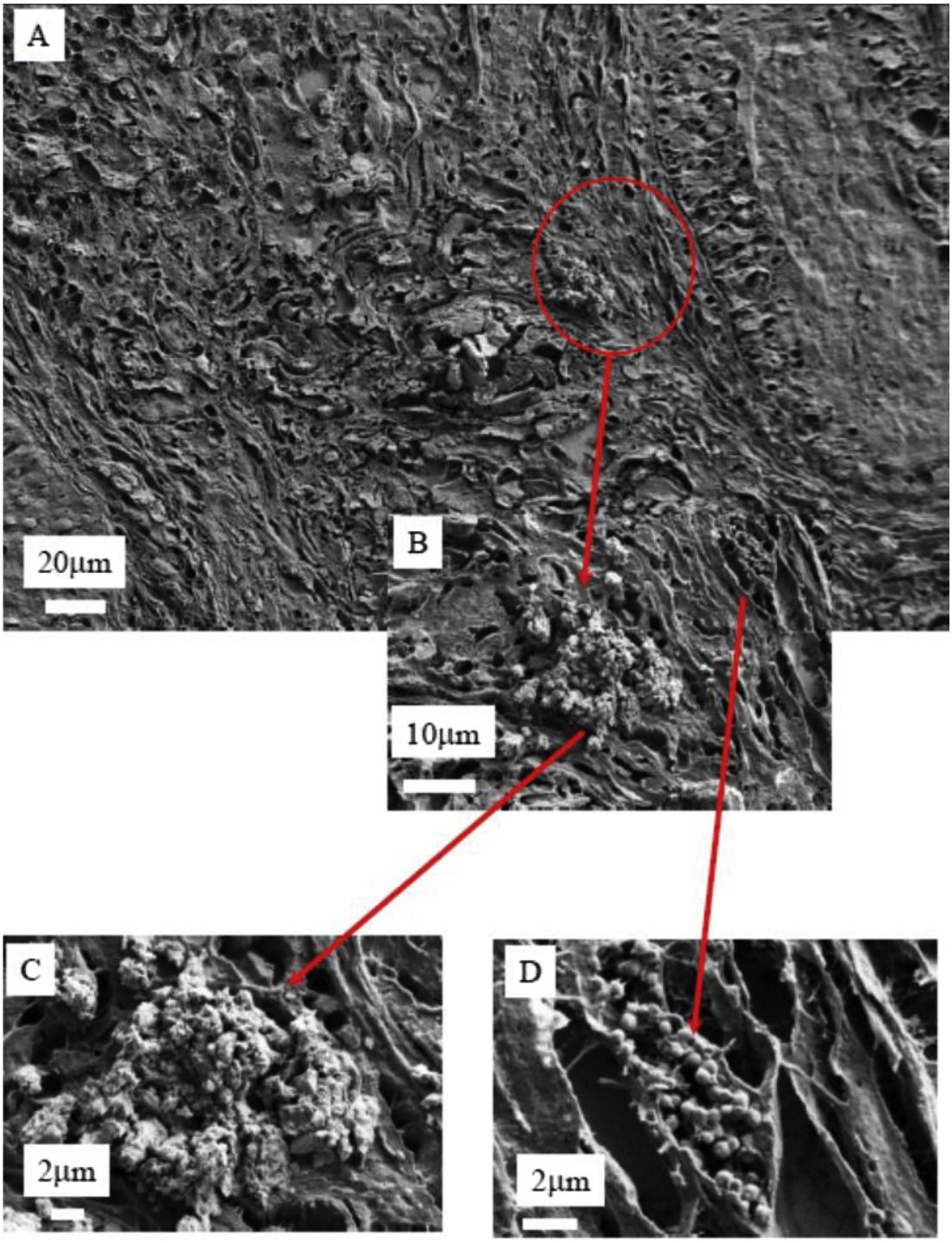

Fig. 9. (A), (B), (C) and (D) SEM photographs of sample No. 3 at different magnifications.

are shown in Figs. 6–8. In summary, in these three samples a mineral deposit was observed within a granuloma, all containing silicium but with a different morphological pattern. In the second sample (Figs. 6 and 7) the deposits were sharp unique irregular objects more than 10 μm long. In the third sample (Fig. 8) the deposit was an aggregate of very small objects some of them at the nanoparticle scale (<0.100 μm). These differences can be explained by the fact that the morphology of the deposits can be modified by the preparation procedure, which can fragment a large single object into small nanoparticles.

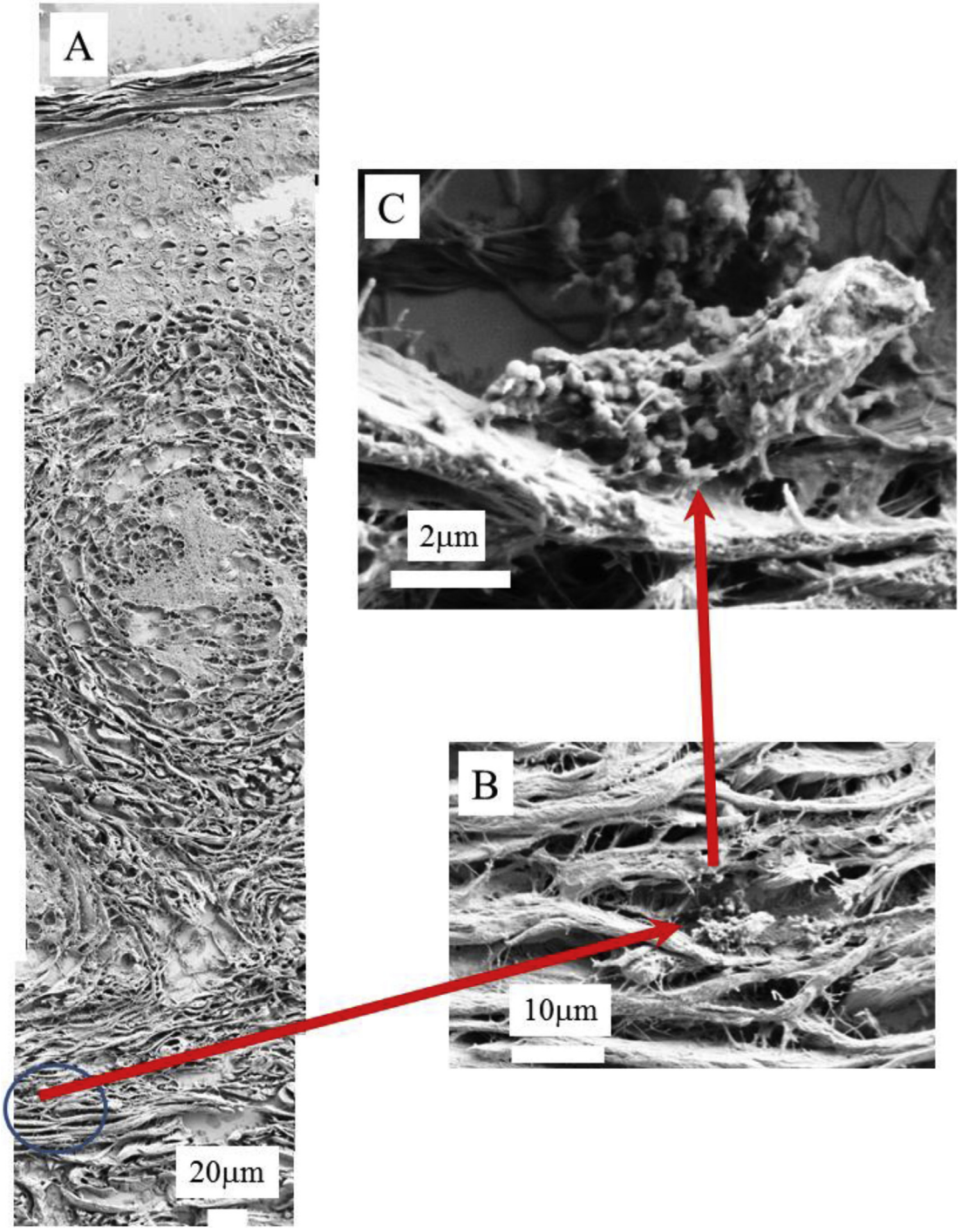

Fig. 10. (A), (B) and (C) SEM photographs of sample No. 5 at different magnifications. In A, we can recognize the three skin layers, the epidermis (50–100 μm), dermis (1–2 mm) and hypodermis (1–2 mm).

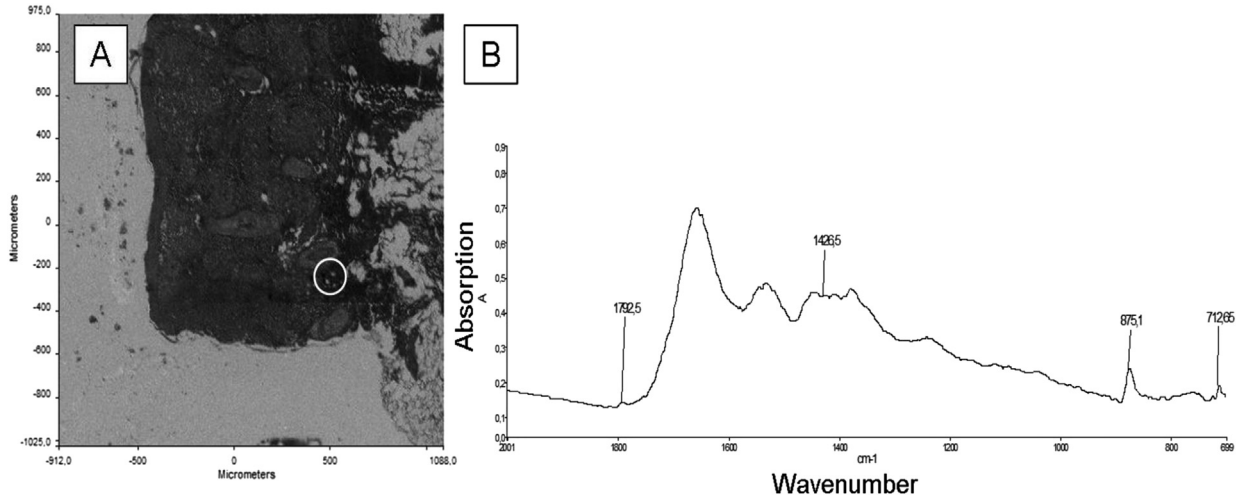

Fig. 11. (A) Optical photograph of sample No. 3; (B) IR spectrum of the peaks characteristic of calcite in a protein matrix, from the area corresponding to the white circle on the map, located in the deep dermis.

3.3.2. Ca carbonate deposits at the periphery of the granulomas

FE-SEM/EDX analysis completes the data from the μFTIR-SEM investigation. Aggregates of submicrometer spherical deposits of Ca carbonate are localized between the collagen fibers (Figs. 9 and 10). Such a spherical morphology may be due to the spray drying technique [37] or analogous methods [38] as described in other organs such as kidney [39,40], breast [41] or cardiovascular tissue [42,43]. Such calcium carbonate nanoparticles are consistent with the spherical morphology of micrometer size calcium carbonate crystallites, as crystallites are composed of a collection of nanocrystals [44].

In order to determine the chemical nature of these spherical entities, μFTIR and EDX were performed. First, μFTIR spectroscopy (Fig. 11) shows that these structures contain a large amount of calcium as confirmed by EDX (Fig. 12). Based on specific IR absorption bands, we can conclude that the spherical entities are calcite. Recall the different calcium carbonate species: anhydrous species ($CaCO_3$), namely calcite, aragonite and vaterite and the hydrated species such as monohydrocalcite ($CaCO_3 \cdot H_2O$) or ikaite ($CaCO_3 \cdot 6H_2O$) and finally amorphous $CaCO_3$ which may contain water molecules [45,46]. From a medical point of view, very few reports discussed tissue calcium carbonate in the context of sarcoidosis. For example, a report by Reid and Andersen [47] mentions the presence of dolomite (not really a true calcium carbonate as its stoichiometric formula is $CaMg(CO_3)_2$). In pancreas, the presence of calcium carbonate (calcite, aragonite, vaterite) has been widely reported [48,49]. Also, otoliths are composed of calcium carbonate and protein [50].

The presence of these abnormal deposits in the skin is one of the striking results of this submission. It is worth emphasizing that those spherical calcium carbonate particles are not refractive, which, together with their very small size, can explain why these deposits were not seen in PLE.

4. Conclusion

The comprehensive set of data from μFTIR and FEDS-SEM/EDX yields the first information on the physico-chemical nature of cutaneous granulomas and peri-granulomas tissues in sarcoidosis patients. Notably only a few granulomas contained silica particles and the possibility that silica may simply be a foreign material either forming a nidus for a granuloma or related to a macrophage contaminant ingested before the granuloma formation. Moreover, calcium carbonate was detected at the periphery

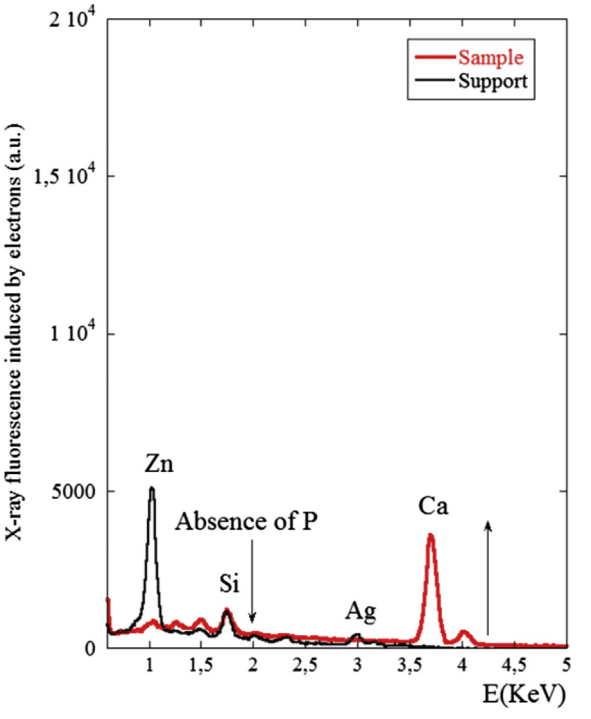

Fig. 12. X-ray fluorescence of the sample No. 3 induced by electrons. The contributions of trace elements coming from the support namely Zn (1.01 keV), Si (1.74 keV) and Ag (2.98 keV) are clearly visible. We can noticed the absence of fluorescence signal coming from P (2.01 keV) and the presence of a significant signal related to Ca (3.7 keV) in line with the FTIR spectrum showing the presence of calcite.

of the granulomas in 4/10 biopsies. The fact that these deposits were located at the periphery of the granulomas, whereas silica was detected in the center, prompts us to think that calcium carbonate is produced by the granulomas, whereas silica contributes to their formation.

Acknowledgements

We are greatly indebted to Profs. Patrice Callard, Isabelle Brochériou and Dr. Claude Bachmeyer for their great help and constant support in this study.

References

[1] R.P. Baughman, A.S. Teirstein, M.A. Judson, M.D. Rossman, H. Yeager Jr., E.A. Bresnitz, L. DePalo, G. Hunninghake, M.C. Iannuzzi, C.J. Johns, G. McLennan, D.R. Moller, L.S. Newman, D.L. Rabin, C. Rose, B. Rybicki, S.E. Weinberger, M.L. Terrin, G.L. Knatterud, R. Cherniak, Am. J. Respir. Crit. Care Med. 164 (2001) 1885.
[2] A. Haimovic, M. Sanchez, M.A. Judson, S. Prystowsky, J. Am. Acad. Dermatol. 66 (2012) 717.
[3] G. Zissel, J. Müller-Quernheim, Clin. Chest Med. 36 (2008) 549.
[4] K.A. Wanat, M. Rosenbach, Clin. Chest Med. 36 (2015) 685.
[5] J.P. Callen, Arch. Dermatol. 137 (2001) 485.
[6] J. Marcoval, A. Moreno, J. Maña, J. Cutan. Pathol. 31 (2004) 516.
[7] N.M. Walsh, J.G. Hanly, R. Tremaine, S. Murray, Am. J. Dermatopathol. 15 (1993) 203.
[8] O.P. Sharma, Curr. Opin. Pulm. Med. 6 (2000) 442.
[9] M. Conron, C. Young, H.L.C. Beynon, Rheumatology 39 (2000) 707.
[10] J.S. Walsh, J.A. Fairley, J. Am. Acad. Dermatol. 33 (1995) 693.
[11] G. Izbicki, R. Chavko, G.I. Banauch, M.D. Weiden, K.I. Berger, T.K. Aldrich, C. Hall, K.J. Kelly, D.J. Prezant, Chest 131 (2007) 1414.
[12] V. Rafnsson, O. Ingimarsson, I. Hjalmarsson, H. Gunnarsdottir, Occup. Environ. Med. 55 (1998) 657.
[13] A. Ostrowski, D. Nordmeyer, A. Boreham, C. Holzhausen, L. Mundhenk, C. Graf, M.C. Meinke, A. Vogt, S. Hadam, J. Lademann, E. Rühl, U. Alexie, A.D. Gruber, Beilstein J. Nanotechnol. 6 (2015) 263.
[14] D. Bazin, M. Daudon, C. Combes, C. Rey, Chem. Rev. 112 (2012) 5092.
[15] D. Bazin, J.-P. Haymann, E. Letavernier, J. Rode, M. Daudon, Presse Méd. 43 (2014) 135.
[16] D. Bazin, M. Daudon, J. Phys. D. Appl. Phys. 45 (2012) 383001.
[17] M. Daudon, D. Bazin, J. Phys. Conf. Ser. 425 (2013) 022006.
[18] F. Brisset, M. Repoux, J. Ruste, F. Grillon, F. Robaut, Microscopie électronique à balayage et Microanalyses, EDP Sciences, 2008.
[19] M. Daudon, D. Bazin, Urolithiasis: Basic Science and Clinical Practice, 2012, p. 683.
[20] D. Bazin, M. Daudon, Ann. Biol. Clin. 73 (2015) 517.
[21] N. Quy-Dao, M. Daudon, Infrared and Raman Spectra of Calculi, Elsevier, Paris, 1997.
[22] E.V. Wilson, M.J. Bushiri, V.K. Vaidyan, Spectrochim. Acta Part A 77 (2010) 442.
[23] A. Dessombz, D. Bazin, P. Dumas, C. Sandt, J. Sule-Suso, M. Daudon, PLoS One 6 (2011) e28007.
[24] I. Faklaris, N. Bouropoulos, N.A. Vainos, Cryst. Res. Technol. 48 (2013) 632.
[25] S. Gràcia-Garcia, F. Millán-Rodríguez, F. Rousaud-Barón, R. Montañés-Bermúdez, O. Angerri-Feu, F. Sánchez-Martín, H. Villavicencio-Mavrich, A. Oliver-Samper, Actas Urológicas Españolas 35 (2011) 354.
[26] M. Pucetaite, S. Tamosaityte, A. Engdahl, J. Ceponkus, V. Sablinskas, P. Uvdal, Central Eur. J. Chem. 12 (2014) 44.
[27] F. Blanco, P. Ortiz-Alías, M. López-Mesas, M. Valiente, J. Biophot. 8 (2015) 457.
[28] A. Dazzi, C.B. Pratter, Q. Hu, D.B. Chase, J.F. Rabolt, C. Marcott, Appl. Spectr. 66 (2012) 1365.
[29] C. Policar, J.B. Waern, M.A. Plamont, S. Clède, C. Mayet, R. Prazeres, J.-M. Ortega, A. Vessières, A. Dazzi, Angew. Chem. Int. Ed. 50 (2010) 860.
[30] A. Dazzi, R. Prazeres, F. Glotin, J.-M. Ortega, M. Alsawaftah, M. de Frutos, Ultramicroscopy 108 (2008) 635.
[31] K. Belbachir, R. Noreen, G. Gouspillou, C. Petibois, Anal. Bioanal. Chem. 395 (2009) 829.
[32] C. Marcott, M. Lo, K. Kjoller, Y. Domanov, G. Balooch, G.S. Luengo, Exp. Dermatol. 22 (2013) 419.
[33] E.R. Lippincott, A. Van Valkenburg, C.E. Weir, E.N. Bunting, J. Res. Natl. Bureau Stand. 61 (1958) 2885.
[34] Y. Liang, C.R. Miranda, S. Scandolo, J. Chem. Phys. 125 (2006) 194524.
[35] R.W.G. Wychoff, Crystal Structures, 2nd ed., Vol. 1, Krieger, Malabar, FL, 1982 one useful website is, http://cst-www.nrl.navy.mil/lattice/.
[36] K.M.A. O'Reilly, R.P. Phipps, ThH. Thatcher, B.A. Graf, J. Van Kirk, P.J. Sime, Am. J. Physiol. Lung Cell. Mol. Physiol. 288 (2005) L1010.
[37] E. Lugscheider, M. Knepper, K.A. Gross, J. Therm. Spray Technol. 1 (1992) 215.
[38] M. Aizawa, T. Terado, F.S. Howell, K. Itatani, Mater. Res. Bull. 34 (1999) 1215.
[39] D. Bazin, G. André, R. Weil, G. Matzen, E. Veron, X. Carpentier, E. Veron, Urology 79 (2012) 786.
[40] K.M. Englert, J.A. McAteer, J.E. Lingeman, J.C. Williams, Urolithiasis 41 (2013) 389.
[41] A.S. Haka, K.E. Shafer-Peltier, M. Fitzmaurice, J. Crowe, R.R. Dasari, M.S. Feld, Cancer Res. 62 (2002) 5375.
[42] K. Schmid, W.O. McSharry, C.H. Pameijer, J.P. Binette, Atherosclerosis 37 (1980) 199.
[43] S. Bertazzo, E. Gentleman, K.L. Cloyd, A.H. Chester, M.H. Yacoub, M.M. Stevens, Nat. Mater. 12 (2013) 576.
[44] M. Van Meerssche, J. Feneau-Dupont, Introduction à la Cristallographie et à la Chimie Structurale, Vander, Louvain, Cesson, 1973.
[45] T. Yong-Jin Han, J. Aizenberg, Chem. Mat. 20 (2008) 1064.
[46] Y. Politi, R.A. Metzler, M. Abrecht, B. Gilbert, F.H. Wilt, I. Sagi, L. Addadi, S. Weiner, P.U.P.A. Gilbert, PNAS 105 (2008) 17362.
[47] J.D. Reid, M.E. Andersen, Am. J. Clin. Pathol. 90 (1988) 545.
[48] Y. Itou, T.R. Kataoka, S. Takashima, Eur. J. Radiol. Extra 71 (2009) e65.
[49] I. Matsuda, H. Hao, M. Zozumi, M. Koishi, T. Matsumoto, N. Kaibe, Y. Fujiwara, M. Sasako, S. Hirota, Pathol. Res. Pract. 206 (2010) 372.
[50] R. Oka, T. Okai, H. Kitakata, T. Ohta, Gastrointest. Endosc. 56 (2002) 939.